

The 0.8 to 14.5 μ m Spectral Energy Distributions of Mid-L to Mid-T Dwarfs

D.C. Stephens*, S.K. Leggett[†], Mark S. Marley**, D. Saumon[‡], Michael C. Cushing[§], T.R. Geballe[†], D.A. Golimowski[¶], Xiaohui Fan^{||} and K.S. Noll[¶]

*BYU Department of Physics and Astronomy, N486 ESC, Provo, UT 84602

[†]Gemini Observatory, Northern Operations Center, 670 N. A'ohoku Place, Hilo, HI 96720

^{**}NASA Ames Research Center, MS 245-3, Moffett Field, CA 94035

[‡]Los Alamos National Laboratory, PO Box 1663, MS F663, Los Alamos, NM 87545

[§]Institute for Astronomy, University of Hawaii, 2680 Woodlawn Drive, Honolulu, HI 96822

[¶]Space Telescope Science Institute, 3700 San Martin Drive, Baltimore, MD 21218

^{||}Steward Observatory, University of Arizona, Tucson, AZ 85721

Abstract. We fit theoretical model atmospheres to the spectral energy distribution of 21 L and T dwarfs recently observed with the *Spitzer Space Telescope* to identify and isolate four key physical parameters used in the model characterization of their atmospheres. The wide range of wavelengths observed (~ 0.6 to $14.5 \mu\text{m}$) lets us constrain almost independently the four model parameters used to describe these photospheres: effective temperature (T_{eff}), grain sedimentation (f_{sed}), vertical gas transport efficiency (K_{zz}), and gravity. We find that the ratio of the mid-infrared to near-infrared flux is a good indicator of T_{eff} , while the slope in the near-infrared is strongly dependent on f_{sed} . The CH₄ bands found at 2, 3 and 8 μm are sensitive to the timescale for vertical mixing, and gravity will influence the flux at 2 μm .

Keywords: stars:low-mass, brown dwarfs; stars:fundamental parameters

PACS: 97.20.Vs

INTRODUCTION

Unlike stars, brown dwarfs have spectral energy distributions (SEDs) that evolve through multiple spectral types as they age and cool. While the M to L transition is likely dominated by decreasing effective temperature (T_{eff}), the L to T transition is probably a more complicated consequence of other factors. [1] and [2] have shown that T_{eff} is roughly constant among the late-L and early-T dwarfs. Thus it must be the range of different gravities, metallicities, rotation rates, condensate grain sizes, etc., that produce the large variations in color, opacity, and cloud dynamics observed for the late-L and early-T dwarfs[3]. These different parameters significantly influence the SED of each dwarf, and thus its spectral type. By comparing the SED of L and T dwarfs with those generated from theoretical models, we can investigate the extent to which these variations influence the observed spectra. In so doing, we increase our understanding of cool brown dwarfs and begin to untangle the complex physics of their atmospheres.

In this paper, we discuss new observations from 5.2–14.5 μm that were obtained for 14 late-L and T dwarfs using the *Spitzer Space Telescope*[4]. We use these spectra, augmented with similar spectra of seven mid-L to early-T dwarfs published previously by [5], and our model atmospheres to investigate the influence of four different physical

parameters on the SED of the late-L and early-T dwarfs. For each of these objects near-infrared (1.0–2.5 μm) spectra exist and are used to supplement the mid-infrared data. This combined spectra covers a large wavelength range and provides a better opportunity to untangle the various effects of T_{eff} , gravity, sedimentation efficiency, and vertical mixing. The next sections of the paper introduce the observed objects, the theoretical models that were fit to the data, the fitting procedure that was followed, and the results of our analysis. Due to page limitations we present only the most basic results here, and refer the reader to [6] for the full observational details and results.

OBSERVATIONS

Spectra from 5.2–14.5 μm were obtained for 14 L and T dwarfs using the Infrared Spectrograph (IRS[7]) on the *Spitzer Space Telescope*. The data were supplemented with existing red and near-infrared spectra from \sim 0.6–2.5 μm to extend the range of wavelengths used in the comparison of the data with synthetic spectra. To partially fill the gap between the near- and mid-infrared data, new 3.0–4.1 μm spectra for five of the brighter L-T transition dwarfs was obtained with the Near InfraRed Imager and Spectrograph (NIRI[8]) on the Gemini North Telescope. In addition to these dwarfs, we augmented the sample with similar spectra of seven mid-L to early-T dwarfs observed by [5]. These objects were added to the sample to explore how the inclusion of a vertical mixing parameter, which was not available at the time that the analysis by [5] was performed, would alter the selection of the best model parameters for each dwarf. Details regarding the data acquisition and reduction for the 14 L and T dwarfs and the seven additional dwarfs presented here can be found in [6] and [5] respectively.

A total of 21 L and T dwarfs ranging in spectral type from L3.5 to T5.5 were analyzed in this study and are listed in Table 1. This table provides basic information about the spectral type, relative color, and model parameters that best fit the observed spectra. Throughout this paper we will refer to individual dwarfs by their abbreviated coordinates and refer the reader to Table 1 for their official designation. In this paper we adopt the near-infrared spectral classifications of [9] and [10] for the L and T dwarfs, respectively. The far-optical classifications of [11] for the L dwarfs are included in Table 1 for reference.

MODEL ATMOSPHERES

Synthetic spectra from 0.8–15.0 μm were created from advanced atmosphere models developed by [3]. These models contain four adjustable parameters: T_{eff} , gravity, a cloud sedimentation parameter (f_{sed}), and a parameter that characterizes vertical mixing in the atmosphere (K_{zz}). The models reflect solar metallicity and span parameter ranges appropriate for late-L and T dwarfs: $900 \leq T_{\text{eff}} \leq 1800$ K, with $\Delta T_{\text{eff}} = 100$ K; $g = 300$, 1000, and 3000 m s^{-2} (or $\log g = 4.477$, 5.0, and 5.477 in cgs units); $f_{\text{sed}} = 1, 2, 3, 4$, and ∞ (no clouds); and $K_{zz} = 0$ (no vertical mixing), 10^2 , 10^4 , and $10^6 \text{ cm}^2 \text{s}^{-1}$.

The models include two unique parameters. The first is called f_{sed} , and it describes the efficiency of condensate sedimentation relative to turbulent mixing[12][13]. Basically

TABLE 1. L and T dwarfs observed with *Spitzer* IRS and their best fit model parameters

Name	Sp. Type (IR/Opt)	J-K (MKO)	Relative color	T _{eff} (K)	log g	f _{sed}	K _{zz} (cm ² /s)
2MASS J22443167+2043433	L7.5/L6.5	2.43	very red	1200	5.5	1	10 ⁴
SDSS J115553.85+055957.5	L7.5	1.54	normal	1500	5.0	2	10 ²
SDSS J085758.44+570851.4	L8/L8	1.86	red	1100	4.5	2	10 ⁶
SDSS J133148.88–011652.5	L8/L6	1.25	blue	1500	5.0	3	10 ⁴
2MASS J09083803+5032088	L9/L5	1.51	normal	1400	5.0	2	10 ⁴
SDSS J080531.83+481233.1	L9.5/L4	1.10	blue	1600	5.0	3	0
SDSS J120747.17+024424.8	T0/L8	1.22	normal	1300	5.0	3	0
SDSS J152039.82+354619.8	T0	1.45	normal	1400	5.0	2	10 ²
SDSS J151643.00+305344.3	T0.5	1.67	red	1000	5.5	2	10 ⁴
SDSS J105213.50+442255.6	T0.5	1.43	normal	1200	5.0	3	10 ⁶
SDSS J075840.32+324723.3	T2	0.91	normal	1000	4.5	3	10 ⁴
2MASS J22541892+3123498	T4	−0.02	normal	1300	4.5	nc	0
SDSS J000013.54+255418.6	T4.5	−0.09	normal	1200	4.5	nc	10 ²
SDSS J111009.99+011613.0	T5.5	0.07	very red	1000	4.5	4	10 ⁴
2MASS J22244381–0158521*	L3.5/L4.5	1.92	red	1500	4.5	1	10 ²
2MASS J00361617+1821104	L4/L3.5	1.26	blue	1700	5.0	3	0
2MASS J15074769–1627386	L5.5/L5	1.41	blue	1600	5.0	3	10 ⁴
2MASS J08251968+2115521	L6/L7.5	1.96	red	1100	4.5	2	10 ⁶
DENIS-P J025503.3–470049	L9/L8	1.54	normal	1300	5.0	2	10 ⁴
SDSS J125453.90–012247.5	T2	0.82	normal	1100	4.5	4	10 ⁶
2MASS J05591914–1404488	T4.5	−0.16	normal	1200	4.5	nc	10 ²

* These seven objects are from [5]

larger values of f_{sed} imply larger particle sizes, greater sedimentation efficiency, and thinner clouds; while smaller values of f_{sed} imply the opposite. The second parameter accounts for vertical transport in the atmosphere. It is parameterized in these models by an eddy diffusion coefficient K_{zz} (cm² s^{−1}) that is related to the mixing time scale. Generally, larger values of K_{zz} imply a greater enhancement of CO and N₂ over CH₄ and NH₃ in the upper atmosphere. Values of $\log K_{zz} = 2–6$, correspond to mixing time scales of ~ 10 yr to ~ 1 h.

Ultimately f_{sed} and the strength of vertical mixing above the radiative-convective boundary will depend on the fundamental characteristics of a given dwarf, including temperature, gravity, and metallicity. For now we consider each model parameter to be mutually independent with the goal of understanding how cloud sedimentation and vertical mixing are related to the fundamental properties of the ultracool dwarfs.

FITTING MODELS TO THE OBSERVATIONS

Using the ranges for T_{eff} , $\log g$, f_{sed} , and K_{zz} listed above, we created more than 600 synthetic spectra with flux densities F_V extending from 0.8 to 15.0 μm. These synthetic spectra were initially compared with the objects in Table 1 using a fitting procedure

similar to that described by [5]. This procedure uses a chi-squared statistic to identify the synthetic spectra whose flux density most closely resembles that of the observed spectrum. Multiple fits to the spectra of each object are made, some of which include the entire wavelength range in the fitting, while others focus on limited spectral regions. This typically produces a list of several models that can match the observed flux density equally well within the uncertainties of the data and the models. The task then remains to determine which of these models is the best representation of the data.

In comparing the best-fitting spectra with the observed data, we found that we could fine-tune the parameters T_{eff} , $\log g$, f_{sed} , and K_{zz} almost independently of each other by looking at different spectral regions and identifying which parameters have the largest to smallest effects on the synthetic spectra in those regions. In this way we were able to find the one model whose combined parameters best reproduced the observed data over the object's entire spectral range. Figure 1 illustrates this process for the T0 dwarf, SDSS 1520+35 whose spectra is represented by the solid black curves. The red dashed curve at the top of the figure corresponds to the final best fit model to SDSS 1520+35. The other four blue dashed curves illustrate the steps taken to identify the best model.

We first constrained T_{eff} by examining the ratio of the near- and mid-infrared fluxes, as seen in the top two spectra. Increasing T_{eff} in steps of 100 K significantly reduces the mid-infrared flux relative to the near-infrared flux. Next, we use the slope of the 1.0–2.5 μm flux to determine f_{sed} to ± 1 . Increasing f_{sed} produces a shallower 1.0–2.5 μm slope, as seen from the top and middle spectra. Then we use the strength of the K -band flux to constrain $\log g$ to ± 0.5 dex. Decreasing $\log g$ leads to a brighter K -band, as seen in the spectra at the top and second from the bottom. Finally, we determine K_{zz} to ± 2 dex from the strengths of the CH_4 absorption bands centered at 2.2 μm , 7.65 μm , and, in those cases where L -band spectra are available, 3.3 μm . Table 1 list the model parameters selected for each dwarf using this technique.

RESULTS

The model spectra selected through this technique fit the data very well, which is remarkable given the complexity of their atmospheres. The only exceptions occur for the very red L3.5 dwarf 2MASS 2224-01, the very red L7.5 dwarf 2MASS 2244+20, and the T2 dwarf SDSS 0758+32. The fits to the very red L dwarfs lie at the lower end of our range of f_{sed} , so it is not altogether surprising that our models cannot yet reproduce such dusty atmospheres. Exploratory modeling suggests that the very red L dwarfs may have smaller particle sizes than those predicted by our baseline cloud model, even for $f_{\text{sed}} = 1$. The T2 dwarf is actually better fit by an 1100 K + 800 K binary model, and may be an unresolved binary system. Images of all the spectra and their best fitting models can be found in [6].

In Table 1 we see a clear correlation between the $J - K$ colors of the L dwarfs and the sedimentation efficiency of the clouds. The blue dwarfs are always best fit by the less cloudy atmosphere models ($f_{\text{sed}} = 3$), while the redder dwarfs are best fit by models with $f_{\text{sed}} = 1$ or 2. L dwarfs with neutral colors have f_{sed} values of 2, and the early T dwarfs have f_{sed} values of 3 to 4. The mid-T dwarfs are best fit by a no cloud model, except for the very red T5.5 dwarf SD 1110+01, whose color is mostly likely due to non-solar

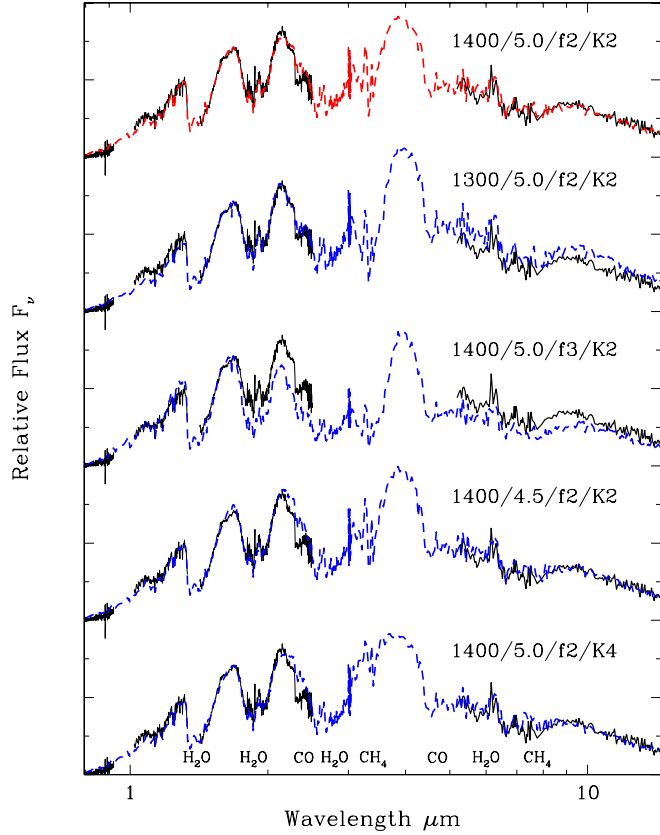


FIGURE 1. Effects on the model fits to the observed spectrum of the T0 dwarf SDSS 1520+35 (solid black curves) as the model parameters are varied. The topmost spectra show the adopted best-fitting model (red dashed curve) with the indicated values of $T_{\text{eff}} / \log g / f_{\text{sed}} / \log(K_{zz})$. The other model spectra (blue dashed curves) demonstrate the effect of changing each parameter in our parametric grid. The labeled values of $\log g = 4.477$ and 5.477 are rounded off to 4.5 and 5.5 respectively. For ease in identifying each parameter, we label the f_{sed} parameters $1, 2, 3$, and 4 , as $f1, f2, f3$, and $f4$. The vertical mixing coefficients are given as K2, K4, and K6 where $\log_{10}(K_{zz}) = 2, 4$, and 6 respectively. The spectra are normalized at $5.4 \mu\text{m}$ and vertically offset for clarity. The model spectra have been smoothed to match the resolution of the observed spectra.

metallicity. These trends are consistent with the finding of [3] that differences in cloud opacity, and not gravity alone, account for the $J - K$ color variations of the L dwarfs.

Comparison of the results found for the seven dwarfs from [5] suggests that those models that include vertical mixing do a better job of reproducing the $2.9\text{--}4.1 \mu\text{m}$ spectral region where the fundamental CH_4 band is located. We find that the T_{eff} values derived for the seven dwarfs by [5] are all warmer by $\sim 100 \text{ K}$ than our corresponding values. For the mid-L to mid-T dwarfs, this discrepancy is probably caused by the need to decrease the CH_4 abundance in the models that lack vertical mixing. Increasing T_{eff} also requires changes in f_{sed} and $\log g$ to better match the modeled and observed spectra. Because our observations and analysis strongly suggest that vertical mixing occurs in cool dwarf atmospheres, we believe that the model parameters found here are superior to those of [5]. Nevertheless, the differences between the two sets of parameters are

within the quoted uncertainties.

CONCLUSIONS

We used the models of [3] to generate and fit synthetic spectra to the red through mid-infrared spectra of 21 L and T dwarfs. These dwarfs have spectral types from L3.5 to T5.5, and some have unusual near-infrared colors. The models generally reproduce the observed spectra well. Four model parameters - effective temperature (T_{eff}), surface gravity ($\log g$), grain sedimentation efficiency (f_{sed}), and a vertical gas transport coefficient (K_{zz}) - were varied in the process of fitting each spectrum. We find that for L and T dwarfs, T_{eff} can be determined from the ratio of the near- to mid-infrared fluxes. The slope of the near-infrared flux distribution can constrain the f_{sed} parameter, and the strengths of the CH₄ bands centered at 2.2, 3.3, and 7.65 μm characterize K_{zz} . Finally, for an assumed metallicity, $\log g$ can be constrained by the 2 μm flux.

The quantity and quality of our spectra, as well as the complexity and reliability of our model atmospheres, represent huge advances in substellar astronomy over the last few years. The observational advances are largely due to the success of the *Spitzer Space Telescope*. The models should continue to improve as the dependencies on metallicity and grain sizes are investigated.

REFERENCES

1. D. A. Golimowski et al., *aj* **127**, 3516 (2004)
2. F. J. Vrba et al., *aj* **127**, 2948 (2004)
3. D. Saumon, and M. S. Marley, *apj*, submitted (2008)
4. M. W. Werner et al., *apjs* **154**, 309 (2004)
5. M. C. Cushing et al., *apj* **678**, 1372 (2008)
6. D. C. Stephens et al., *apj*, submitted (2008)
7. J. R. Houck et al., *apjs* **154**, 18 (2004)
8. K. W. Hodapp et al., *pasp* **115**, 1388 (2003)
9. T. R. Geballe et al., *apj* **564**, 466 (2002)
10. A. J. Burgasser, T. R. Geballe, S. K. Leggett, J. D. Kirkpatrick, and D. A. Golimowski, *apj* **637**, 1067 (2006)
11. J. D. Kirkpatrick et al., *apj* **519**, 802 (1999)
12. A. S. Ackerman, and M. S. Marley, *apj* **556**, 872 (2001)
13. M. S. Marley, S. Seager, D. Saumon, K. Lodders, A. S. Ackerman, R. S. Freedman, and X. Fan, *apj* **568**, 335 (2002)